

## Measurement of hot-electron scattering processes at Au/Si(100) Schottky interfaces by temperature-dependent ballistic-electron-emission microscopy

C. A. Ventrice, Jr., V. P. LaBella, G. Ramaswamy,\* H.-P. Yu, and L. J. Schowalter  
*Department of Physics, Rensselaer Polytechnic Institute, Troy, New York 12180*

(Received 31 July 1995)

Ballistic-electron-emission microscopy measurements have been performed on *n*-type Au/Si(100) interfaces for injection energies up to 1.2 eV over a range of Au overlayer thicknesses from  $\sim 65$  to  $\sim 340$  Å at both room temperature and 77 K. Hot-electron attenuation lengths in the Au overlayer have been determined to be  $133 \pm 2$  Å at room temperature and  $147 \pm 6$  Å at 77 K over the energy range of 0.92–1.20 eV above the Fermi level. The lack of energy dependence and the relatively small temperature-dependent change in the attenuation lengths that have been measured indicate that electron scattering with defects is the dominant mechanism affecting hot-electron transport in these Au overlayers. The ratio of the zero-thickness collection current at 77 K to that at room temperature has been measured to be  $1.79 \pm 0.09$ . This large increase in the collection efficiency at 77 K is attributed primarily to the large temperature dependence of the transverse acoustic-phonon population in Si. Images with significant reductions in the collection current at topographic locations that have a large surface gradient have been obtained at room temperature. Calculations, which assume that the probability of transmission across the interface is independent of the transverse momentum of the electron, correlate well with the experimentally observed reductions. This result indicates that the injected electrons remain forward focused with little broadening as they pass through the Au overlayer, which implies that elastic scattering at the Au/Si interface accounts for the observation from previous Au/Si ballistic-electron-emission microscopy studies that transverse momentum is not conserved.

### I. INTRODUCTION

A fundamental understanding of the various hot-electron scattering processes at metal-semiconductor (*M-S*) interfaces is important for the optimization of the transport properties of many electronic devices such as metal-base transistors and infrared Schottky photodiodes. During the initial stages of the development of solid-state technology in the 1960s, there was considerable research effort in this field. The primary experimental method which was used to measure the scattering lengths of hot electrons in metals during that time was internal photoemission.<sup>1</sup> This technique measures the photoresponse of a *M-S* interface over a series of metal film thicknesses to determine the attenuation length  $\lambda_a$  of the photoexcited electrons. However, extracting the path length for inelastic scattering from these data is complicated by the fact that the penetration depth of the photons in the metal as well as the energy distribution of the photoexcited electrons is dependent on the photon energy. In addition, the kinetic-energy range over which  $\lambda_a$  can be measured is limited to the band gap  $E_g$  of the semiconductor. The uncertainty in these early internal photoemission measurements is exemplified by the fact that values of  $\lambda_a$  ranging from 740 to 330 Å at a photon energy of  $\sim 1$  eV have been reported for Au/Si samples by different research groups.<sup>2-4</sup>

The development of ballistic-electron-emission microscopy (BEEM) by Bell and Kaiser<sup>5</sup> has provided the scientific community with a powerful tool for determining hot-electron scattering lengths at *M-S* interfaces. BEEM is a scanning-tunneling-microscopy (STM)-based technique where the STM tip is used as a very narrow, energy-tunable, forward-focused source for electron injection into a metal overlayer.

By collecting the current which passes through the metal into the semiconductor as a function of tip position and tip bias, information about the local Schottky-barrier height and the hot-electron transport properties can be obtained on a nanometer scale. However, to properly interpret the spectroscopy data and interfacial images obtained with BEEM, a fundamental understanding of the scattering process within the metal overlayer, at the metallurgical interface, and within the Si substrate, is essential. In this paper, we report BEEM measurements which were performed to determine the relative importance of temperature-dependent scattering mechanisms on hot-electron transport across Au/Si(100) interfaces. The Au/Si system was chosen as a model *M-S* interface primarily because of the relatively simple electronic structure of Au, a lone 6*s* electron in its outer shell and a filled inner 5*d* shell. In addition, Au is a noble metal which provides an advantage over most metals in that it can be characterized under ambient conditions.

Although Au/Si has been the most thoroughly studied interface with the BEEM technique, it has also proved to be one of the most controversial interfaces. In the first BEEM studies of Au/Si(100) by Bell and Kaiser,<sup>5</sup> excellent agreement was obtained between their spectroscopy data and calculated curves which were derived assuming ballistic transport through the metal overlayer and transverse momentum conservation at the interface. However, Schowalter and Lee<sup>6</sup> made the observation that the BEEM spectra for both the Si(100) and Si(111) substrates have similar line shapes and current onsets, which is unexpected since transport into the Si(111) surface requires a large transverse crystal momentum component while transport into the Si(100) surface does not. Monte Carlo simulations of the BEEM spectra using a model

which conserves transverse momentum at the  $M$ - $S$  interface were performed, and indicated that elastic scattering in the Au overlayers, accompanied by multiple reflections off the surface and interface, resulted in a near-isotropic momentum distribution and an inherent loss of spatial resolution at the  $M$ - $S$  interface. A subsequent BEEM study by Lee *et al.*,<sup>7</sup> which found no correlation between surface gradients and the measured BEEM current, gave support to these Monte Carlo calculations. In contrast to these results, a BEEM study by Palm, Arbes, and Schulz<sup>8</sup> which directly imaged fluctuations in the Schottky-barrier height of Au/Si(100) interfaces over spatial distances of  $\sim 15$  Å provides evidence that transport through the metal overlayer is essentially ballistic.

To complicate matters further, a microscopy study by Fernandez *et al.*<sup>9</sup> found that for Au/Si interfaces grown under ultrahigh-vacuum (UHV) conditions on bare Si and imaged in air, no BEEM current could be detected. They interpreted the lack of BEEM current to the formation of a disordered Au-Si alloy at the interface, which resulted in strong scattering of the BEEM electrons. In addition, they found that by controllably dosing the clean Si surface with various gas molecules before Au deposition, they could obtain homogeneous BEEM currents that could be irreversibly changed by performing BEEM at tip biases higher than  $\sim 3$  V. However, a recent BEEM study by Cuberes *et al.*<sup>10</sup> of Au/Si(111) samples prepared and imaged under UHV conditions found that BEEM currents could be obtained at tip biases as large as 8 eV with no apparent modification of the interface. Their synchrotron-based photoelectron spectroscopy (PES) results also indicated that the Au/Si interface formed at room temperature (RT) is an abrupt interface with a silicidelike surface segregation layer. Trying to reconcile these results is difficult due to differences in sample preparation conditions and in the methods of detection used by many of the groups performing BEEM research.

Although the experimental evidence for nonconservation of transverse momentum is quite strong for Au/Si (Ref. 6) and Pd/Si (Ref. 11) interfaces, the precise nature of the scattering mechanisms is not well understood. It would seem that symmetry breaking parallel to the interface would be a sufficient condition for violation of transverse momentum conservation, since these are nonepitaxial systems. On the other hand, microscopy and spectroscopy studies of Au/GaP(110) (Ref. 12) and Mg/GaP(110),<sup>12,13</sup> which are nonepitaxial and also nonabrupt interfaces, have obtained good agreement between curves fitted with a transverse momentum-conserving model and their experimental data. Presently, it is not clear whether these discrepancies result from an additional source of scattering that may be present at Au/Si and Pd/Si interfaces or from the method which was used to model the data for the Au/GaP(110) and Mg/GaP(110) studies.

To better understand the scattering mechanisms at Au/Si interfaces, we have performed a temperature-dependent BEEM spectroscopy and RT BEEM microscopy study on the Au/Si(100) interface. Our spectroscopy data indicate that there is a large temperature dependence on the measured BEEM transmittance, yet only a small temperature-dependent change in the attenuation length of the electrons in the Au overlayers. From these results, we have determined that the primary temperature-dependent scattering mechanism affecting BEEM electron transport is acoustic-phonon

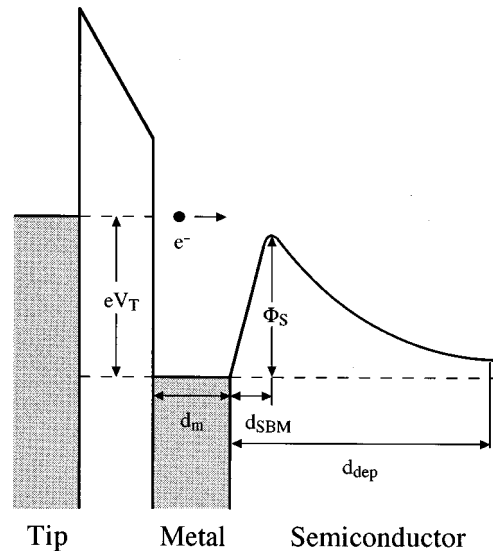


FIG. 1. Schematic of BEEM electron transport across a metal-semiconductor Schottky interface (not drawn to scale). For electrons injected into the metal overlayer with a tip bias greater than the Schottky barrier,  $\Phi_S$ , a fraction of the injected electrons will travel across the barrier and be detected as a BEEM electron. The magnitude of the BEEM current is strongly influenced by the scattering processes in the metal overlayer, at the metallurgical interface, and within the semiconducting substrate.

absorption in the Si substrate. Within the uncertainty of the measurements of  $\lambda_a$ , no energy dependence was observed at RT or 77 K. This result and the aforementioned relatively small temperature dependence of  $\lambda_a$  indicate that the mean free path for scattering from defects in the Au overlayer is significantly smaller than that for inelastic electron-electron scattering or for electron-phonon scattering. Evidence of reductions in the BEEM current for large surface gradients has been obtained for microscopy images taken with sufficiently sharp STM tips, and this has been correlated with the increase in path length to the interface, assuming that the probability of transmission is independent of the angle of incidence. This result provides strong evidence that electron transport through the Au overlayer is essentially ballistic, and that the observed violation of transverse momentum conservation occurs at the interfacial region.

## II. HOT-ELECTRON SCATTERING PROCESSES

A schematic of BEEM electron transport across a  $M$ - $S$  Schottky interface is shown in Fig. 1. Electrons injected into the metal overlayer from the STM tip will have an energy distribution which decays exponentially from a maximum value of  $eV_T$ . All electrons which approach the semiconductor region with an energy which is less than the Schottky barrier height  $\Phi_S$  will be scattered back into the metal. A fraction of the electrons which approach the semiconducting region with an energy greater than  $\Phi_S$  will travel across the barrier and be detected as a BEEM electron. The magnitude of the collected BEEM current is strongly influenced by scattering mechanisms in the metal overlayer, at the metallurgical interface, and within the semiconducting substrate.

A determination of the relative length scales of elastic and

inelastic scattering processes in the metal overlayer is especially important since these scattering events have a direct effect on the resolution of BEEM at the  $M$ - $S$  interface and limit the range of metal overlayer thicknesses which can be probed. Electrons can scatter elastically off defect sites or quasielastically by emission or absorption of acoustic phonons. For metals with more than one atom per primitive basis, the emission and absorption of optical phonons is also possible (Au has only one atom in its primitive basis). Although the energy quanta of acoustic phonons are typically on the order of a few meV, the energy quanta of optical phonons can exceed 50 meV for compound metals. Therefore, the determination of whether electron scattering with optical phonons is considered to be a quasielastic process depends on the particular modes available for that system. Hot electrons can also undergo inelastic electron-electron collisions with electrons near the Fermi level, resulting in an average energy loss of half of their original kinetic energy. When the inelastic mean free path for scattering,  $\lambda_i$ , is of the same order as the elastic mean free path  $\lambda_e$ , the transport process is essentially ballistic, since electrons which have undergone multiple-scattering events will, on average, not have enough kinetic energy to cross the Schottky barrier. In this limit, the BEEM current  $I_b$  should show a clear exponential dependence on metal film thickness with  $\lambda_a$  measured in a BEEM experiment given by  $1/\lambda_a = 1/\lambda_i + 1/\lambda_e$ . In the limit where  $\lambda_e \ll \lambda_i$ , the transport is expected to be diffusive in nature since the probability of undergoing multiple elastic scattering events before scattering inelastically is high. This will result in an electron momentum distribution at the  $M$ - $S$  interface which is completely independent of the momentum distribution at the point of injection.

At the  $M$ - $S$  interface, a fraction of the incident electrons will backscatter into the metal overlayer due to quantum-mechanical reflection. For nonepitaxial systems and non-abrupt interfaces, there will be a break in symmetry parallel to the interface which will result in additional scattering at the interface. For epitaxial systems, the transverse momentum of the electron is expected to be conserved as it travels from the metal to the semiconductor. This condition will result in a critical angle for transport into the semiconductor substrate which increases as a function of the energy of the incident electron.<sup>5</sup> As a direct consequence of transverse momentum conservation, either a delayed or soft threshold for  $I_b$  is expected for electron transport into semiconductor surfaces where the projection of the conduction-band minimum is not on the surface Brillouin-zone center.

Within the semiconductor substrate, electrons can scatter by emission or absorption of either acoustic or optical phonons. As shown in Fig. 1, the position of the Schottky-barrier maximum is not at the metallurgical  $M$ - $S$  interface but is shifted by a few nanometers into the semiconductor due to the image potential. Electrons with energies just over the threshold for transmission that excite phonons in the region before the Schottky-barrier maximum are expected to have a high probability of reentering the metal. Beyond the Schottky-barrier maximum, the internal electric field in the depletion region accelerates the electrons toward the interior of  $n$ -type semiconductors. Therefore, the effect of phonon scattering on the magnitude of  $I_b$  in the region beyond the Schottky-barrier maximum depends on the doping density of

the semiconductor, since this defines the length of the depletion region, and thus the acceleration rate. For the 2–4- $\Omega$  cm samples used in this experiment, the distance to the Schottky-barrier maximum  $d_{SBM}$  and the depletion depth  $d_{dep}$  are calculated to be  $\sim 50$  Å and  $\sim 1$   $\mu$ m, respectively.<sup>14</sup> Since this is a relatively low doping density, electrons which scatter in the region just beyond the Schottky-barrier maximum are expected to have an equal probability of either reentering the metal or passing through the semiconductor depletion region. Once the kinetic energy of the electrons in the semiconductor exceeds  $E_g$ , electron-hole pair generation, or impact ionization, becomes possible. Since the internal electric field in the semiconductor will sweep the electrons toward the interior of the semiconductor and the hole toward the metal, an electron multiplication process occurs.<sup>15</sup>

For metal overlayers more than a few monolayers thick,  $\Phi_S$ ,  $d_{dep}$  and  $d_{SBM}$  are expected to be coverage independent. Therefore, the BEEM current can be expressed as a product of the transmissivities through the metal overlayer, across the metallurgical interface, and through the semiconductor depletion region. The proportion of electrons which traverse the metal region with energy  $E$  will decay exponentially with the path length to the metallurgical interface,  $d_m/\cos(\theta)$ , where  $\theta$  defines the injection angle from the surface normal. This results in the following expression for the measured BEEM current;

$$I_B(E, T, d_m) = I_{tip} A(E) B(E, T) \exp[-d_m/\lambda_a(E, T) \cos(\theta)], \quad (1)$$

where  $A(E)$  is a kinematic transmission factor for electron transport from the metal overlayer into the semiconductor lattice,  $B(E, T)$  is the transmission factor for electron transport through the semiconductor depletion region, and  $I_{tip}$  is the injected current into the metal overlayer. The factor  $A(E)$  is assumed to be independent of the angle of incidence, which results from the assumption of nonconservation of transverse momentum at the interface.<sup>6</sup> Both  $B(E, T)$  and  $\lambda_a(E, T)$  should be temperature dependent, since the path length for phonon absorption will depend strongly on the phonon populations in the metal and semiconductor regions.

### III. EXPERIMENT

The BEEM measurements were performed with a modified Kaiser-Jaklevic STM design<sup>16</sup> which has three, separate, orthogonal, planar piezo drives for tip control and uses a stepper motor for the fine approach of the sample. The STM is housed in a liquid-nitrogen ( $LN_2$ ) Dewar which is incorporated into a glove box. To perform low-temperature BEEM, the Dewar is purged with high-purity  $N_2$  before backfilling with  $LN_2$ . Although the original design of the STM placed the tip current amplifier and BEEM current amplifier in the Dewar near the STM head to reduce pickup noise, significant changes in the performance characteristics of the operational amplifiers and the feedback resistors were observed when immersed in  $LN_2$ . Since maintaining an amplifier gain which is independent of the temperature of the sample is crucial to measuring the temperature dependence of the BEEM transmissivity, the amplifiers were moved outside of the Dewar into separate die-cast aluminum boxes

which are attached to the STM support flange via standard BNC connectors. Low-temperature compatible ultrathin coax<sup>17</sup> is used to carry the signals to the amplifiers, with the outer conductor biased at the same potential as the inner conductor to reduce capacitive coupling. The outer insulating sheath of the coax was also removed to improve the flexibility of the coax at low temperatures.

The Au/Si(100) Schottky diodes were prepared from *n*-type 2–4- $\Omega$  cm Si. An Ohmic contact was applied to the back of each sample by melting indium onto an area of the sample which had been roughened with a diamond scribe. The quality of the Ohmic contacts made by this method were checked by measuring the resistance across Si samples with indium applied to both the front and back of the sample. Resistance values across these In-Si-In junctions of  $\sim 40$   $\Omega$  at RT were consistently measured. The oxide of the Si was removed by dipping the samples in a solution of 10:1 ethanol:HF solution for 1–2 min. After removal from the etching solution, the samples were dried with high-purity  $N_2$  before insertion into a cryopumped evaporation unit. The Au was evaporated from a tungsten thermal boat source through a shadow mask to form a rectangular  $2.5 \times 10$ -mm<sup>2</sup> diode. The nominal deposition rate was  $\sim 0.5$   $\text{\AA}/\text{s}$ , and was monitored with a quartz-crystal microbalance. The base pressure of the evaporation unit is  $\sim 10^{-8}$  Torr, with a typical evaporation pressure of  $\sim 5 \times 10^{-7}$  Torr. Calibration of the Au overlayer coverages measured with the quartz-crystal microbalance was performed periodically using Rutherford backscattering at a separate facility. The uncertainty in the measurement of the Au overlayer thickness is estimated to be within  $\pm 5\%$ . It is also noted that in the early stages of this study, samples were prepared by applying the indium contact after the deposition of the Au to prevent any effect that solvation of indium in the etching solution might have on the etching procedure. However, this technique often resulted in images with large changes in the BEEM current which could not be correlated to any topographic features. It is assumed that this effect results from interdiffusion of Au and Si during the application of the indium, since a previous Auger electron spectroscopy (AES)/low-energy electron-diffraction (LEED) study<sup>18</sup> and a transmission electron microscopy (TEM) study<sup>19</sup> have provided evidence for gold silicide formation at the *M*-*S* interface at temperatures well below the eutectic of 363  $^\circ\text{C}$ .

Both Au and Pt-Ir (90:10) STM tips were chosen for the BEEM measurements since they do not form a native oxide under ambient conditions. The Au tips were prepared from 0.25-mm-diameter wire either by dc electrochemical etching in a 50:50 HCl:ethanol solution or by cleaving at a very sharp angle with a razor blade. Etching produced very sharp whiskerlike tips, as examined under an optical microscope. However, instabilities in the tunnel current during the fine sample approach were often observed for etched tips which was correlated to the poor mechanical rigidity of the whiskerlike tip structures. Since cleaved tips did not exhibit instabilities during the fine approach, this was the primary method used for making Au tips. The STM images from both etched and cleaved Au tips showed similar topographies. The Pt-Ir tips were prepared from 0.50-mm-diameter wire by cutting the wire at a very sharp angle with ordinary wire snippers. Since previous STM studies with Au tips have shown that Au atoms field desorb at a relatively low tip bias of  $-3.2$

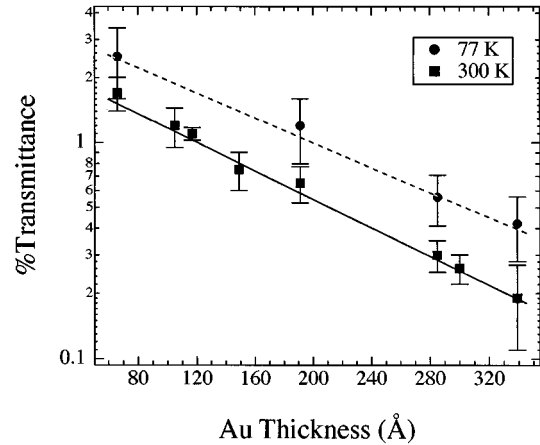


FIG. 2. Semilog plot of BEEM transmittances  $I_B/I_T \times 100$ , at a tip bias of  $-1.2$  V measured on several Au/Si(100) samples at 77 K (circles) and RT (squares). A minimum of 80 spectra were collected at each coverage and temperature. The linear curves through the data sets represents least-squares fits applied to the data. From the slope and intercept of these curves, the attenuation length of the electrons in the Au overlayer,  $\lambda_a$ , and the zero thickness transmittance  $I_0$  are determined.

$V_{20}$ , the energy range for our spectroscopic data was limited to 1.2 eV to stay well below the field desorption limit.

## IV. RESULTS

### A. Temperature-dependent BEEM spectroscopy

BEEM spectroscopy spectra were obtained at both RT and 77 K over a range of Au overlayer thicknesses from  $\sim 65$  to  $\sim 340$   $\text{\AA}$ . A semilog plot of the percent transmittance ( $I_B/I_T \times 100$ ) as a function of Au overlayer thickness at a tip bias of  $-1.2$  V is shown in Fig. 2. A minimum of 80 spectra were collected over a surface area of  $\sim 2000 \times \sim 2000$   $\text{\AA}^2$  for each coverage and temperature. A histogram of the transmittances was plotted for each data set, and the value of the average transmittance was derived by fitting a Gaussian curve to each histogram with the error bars representing the full width at half maximum of the curve. For coverages with both 77-K and RT transmittances, both data sets were collected from the sample within 6 h of each other (the RT data were collected first). The linear curves through the data sets represent least-squares fits applied to the data. Since averaging over such large data sets should eliminate any effects of surface gradient on the transmissivity,  $\lambda_a$  can be obtained from the inverse of the slope of the least-squares fit. The zero length transmittance  $I_0(E, T) = A(E)B(E, T)$  is obtained from the intercept.

The absolute value of  $A(E)$  and  $B(E, T)$  cannot be determined independently from our measurements. However, the temperature dependence of  $B(E, T)$  can be determined by calculating the ratio of the zero length transmittances at 77 K and RT,  $I_0(E, 77 \text{ K})/I_0(E, \text{RT}) = B(E, 77 \text{ K})/B(E, \text{RT})$ , since  $A(E)$  is expected to be independent of temperature. A 50-meV increase in  $\Phi_S$  is measured at 77 K due to the increase in  $E_g$  of Si at low temperatures; therefore, the ratio  $I_0(E, 77 \text{ K})/I_0(E, \text{RT})$  is calculated for constant kinetic energy in the Si conduction band, and is plotted in Fig. 3(a). A value of  $1.79 \pm 0.09$  over a kinetic-energy range of 140–380 meV is

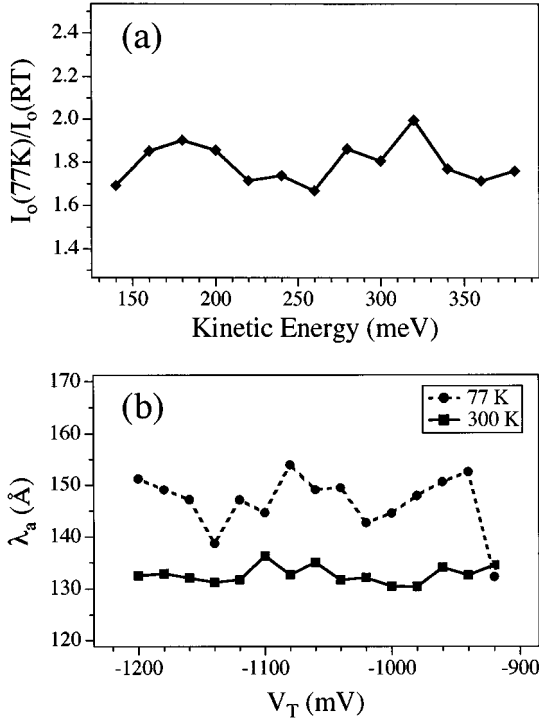


FIG. 3. (a) Plot of the ratio of the zero thickness transmittance at 77 K to that at RT,  $I_0(77\text{ K})/I_0(\text{RT})$ , as a function of kinetic energy,  $eV_T - \Phi_S$ , in the semiconductor. An average value of  $1.79 \pm 0.09$  over the kinetic-energy range of 140–380 meV is obtained for  $I_0(77\text{ K})/I_0(\text{RT})$ . (b) Plot of the attenuation length of the BEEM electrons in the Au overlayer at both 77 K (circles) and RT (squares) as a function of tip bias. Only a slight temperature dependence on  $\lambda_a$  is observed:  $\lambda_a(300\text{ K}) = 133 \pm 2\text{ \AA}$  and  $\lambda_a(77\text{ K}) = 147 \pm 6\text{ \AA}$ . Within the experimental uncertainty of these measurements, no energy dependence of  $\lambda_a$  is observed.

obtained which indicates that approximately half of the electrons which cross into the depletion region at RT backscatter into the metal overlayer after phonon absorption.

A plot of  $\lambda_a$  as a function of tip bias at both RT and 77 K is shown in Fig. 3(b). With our instrumentation,  $\lambda_a$  could be measured accurately down to energies of  $\sim 100$  meV above  $\Phi_S$  over the range of Au thicknesses measured in this study. A value of  $133 \pm 2$  and  $147 \pm 6\text{ \AA}$  were measured for  $\lambda_a$  at RT and 77 K, respectively. As can be seen in Fig. 3(b), no energy dependence for  $\lambda_a$  at either temperature is observed within the uncertainty of the measurements. The value of  $133 \pm 2\text{ \AA}$  that we measure for  $\lambda_a$  at RT deviates slightly from the previously measured values of 125 (Ref. 21) and  $140\text{ \AA}$  (Ref. 22) for Au/Si BEEM measurements. This deviation most likely results from our measurement of  $\lambda_a$  over a larger range of sample thicknesses than in the earlier studies.<sup>21,22</sup> However, differences in the sample preparation procedure and in the uncertainties of the metal overlayer thicknesses may also account for these slight discrepancies. In contrast to these results, an attenuation length of  $\lambda_a = 30\text{ \AA}$  for the system Au/GaP (110) was derived from Monte Carlo simulations of BEEM data.<sup>12</sup> This low value for  $\lambda_a$  is probably an effect of the different growth morphology of Au on GaP (110) over the range of thicknesses measured in their study.

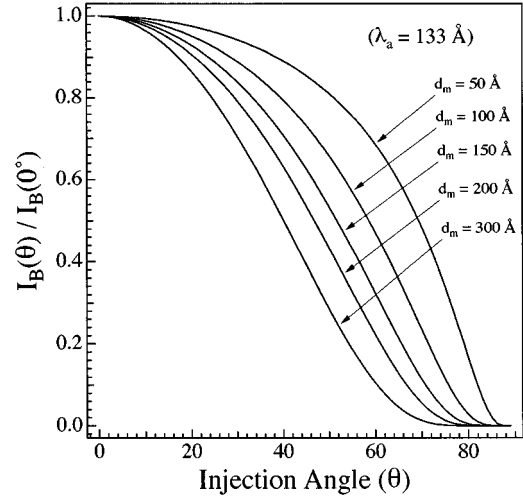


FIG. 4. Calculation of the reduction of normalized BEEM current,  $I_B(\theta)/I_B(0^\circ)$ , that results from the increase in path length to the  $M$ - $S$  interface for nonzero injection angles for several metal overlayer thicknesses. This calculation assumes that any electron reaching the  $M$ - $S$  interface is equally likely to cross it regardless of its momentum parallel to the interface.

### B. Room-temperature BEEM imaging

Although our spectroscopy data, which measured only an 11% increase in  $\lambda_a$  at 77 K, indicate that quasielastic scattering from acoustic phonons in the Au overlayer has a negligible effect on the temperature-dependent transmission probability, this does not preclude the possibility that elastic scattering will affect the trajectory of electrons in the metal overlayer. Therefore, a detailed BEEM microscopy analysis of several Au/Si(100) samples was performed with both Au and Pt-Ir STM tips in an attempt to correlate surface topographic features with changes in the BEEM current. Since electron injection over a surface topographic feature with a nonzero gradient will increase the path length to the  $M$ - $S$  interface, it is expected that reductions in the BEEM current should be observed at large surface gradients. This effect is often called the “search-light effect.” A calculation of the expected reduction in the BEEM current as a function of injection angle is shown in Fig. 4. This calculation assumes that the probability of transmission across the Schottky barrier is independent of the angle of incidence, i.e., transverse momentum is not conserved at the interface. For thin Au overlayers, a very large surface gradient is needed to observe appreciable decreases in  $I_B$  (for a 50- $\text{\AA}$  overlayer, a gradient of  $\sim 70^\circ$  is needed to observe a 50% reduction in  $I_B$ ). At larger Au overlayer thicknesses,  $I_B$  is more sensitive to the surface gradient (for a 300- $\text{\AA}$  overlayer, a gradient of  $\sim 40^\circ$  is needed to observe a 50% reduction in  $I_B$ ), but the magnitude of  $I_B$  is near the limit of detection.

From analysis of our BEEM data measured with Au tips and Pt-Ir tips, it was determined that the tip apex geometry is the primary factor that influences the spatial resolution of BEEM. For imaging with Au tips, changes in the tip geometry were often observed during STM scans and often resulted in featureless images which we correlate to an extremely blunt tip apex. Imaging with Pt-Ir tips produced much more consistent STM topographies. A schematic of the

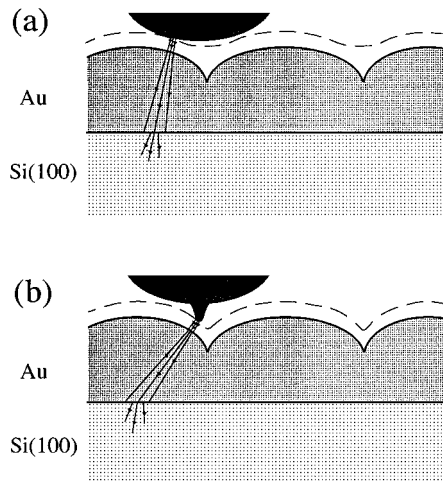


FIG. 5. Schematic of the effect of tip apex geometry on the resolved topography (dashed lines) of the STM and the injection angle of the electrons. (a) Imaging with a tip apex which has a radius of curvature larger than the actual topographic features of the surface will result in an inability to resolve the surface regions with large gradients, e.g., the crevices between the rounded surface structures. (b) Imaging with a tip which has a sharp “minitip” which is longer than the average corrugation height of the surface will result in a measured topography which closely mimics the actual topography.

effect that tip apex geometry has on the resolved surface topography and on the injection angle of the electrons is shown in Fig. 5, where the dashed lines represent the resolved topographies for each tip condition. For the range of Au overlayer thickness in this study, rounded surface features with a spatial extent of  $\sim 50$  to  $\sim 200$  Å and heights from  $\sim 30$  to  $\sim 80$  Å were observed. Since surface gradients large enough to observe appreciable changes in the BEEM current exist only near the bottom of the crevices between these rounded structures, a sharp tip protrusion which is longer than the average height of the rounded surface structures is needed to probe these regions, as shown in Fig. 5(b). A BEEM image of a  $\sim 500 \times \sim 500$ -Å<sup>2</sup> area of a 103-Å Au/Si(100) sample imaged with a Pt-Ir tip is shown in Fig. 6. Asymmetric surface features are observed in the STM topography shown in Fig. 6(a), with surface gradients as large as  $\sim 75^\circ$  being measured. The corresponding BEEM image shown in Fig. 6(b) shows regions of reduced BEEM current of up to  $\sim 85\%$ , which correlate with the regions of the STM topography where high surface gradients were measured. During collection of the data, reductions in the BEEM current were observed for both scan directions, which indicates that this effect does not result from the tracking of the feedback control system. Images performed below the Schottky-barrier height were also featureless, which precludes the possibility that the features observed are due to a coupling of the BEEM current with the signals from the piezoelectric drives.

## V. DISCUSSION

The exponential nature of the transmissivity plots at both 77 K and RT shown in Fig. 2 gives strong evidence that the attenuation length model, Eq. (1), is valid for Au overlayers over the range of  $\sim 65$  to  $\sim 340$  Å. The observation that the

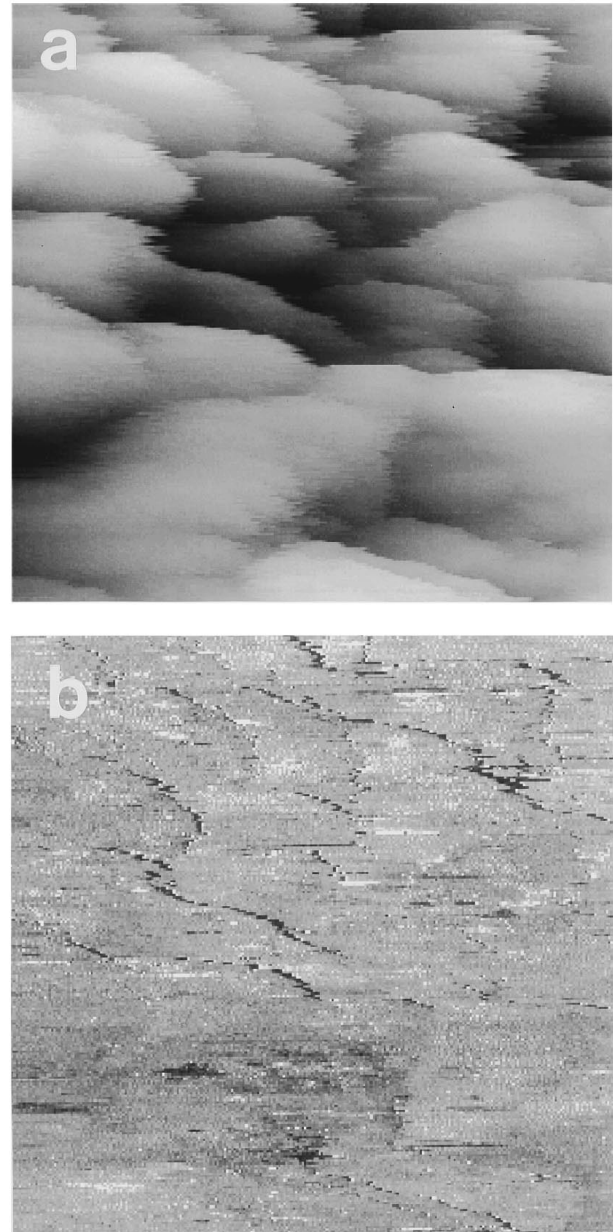


FIG. 6. (a) STM topographic image of a  $\sim 500 \times \sim 500$ -Å<sup>2</sup> area of a 103-Å Au/Si(100) sample ( $V_T = -1.2$  V and  $I_T = 5$  nA). (b) BEEM image taken simultaneously with the topographic image shown in (a). The gray-scale range for the BEEM image is 0–120 pA with dark areas representing low BEEM current. The gray-scale range for the STM image is 120 Å, with light areas representing high surface features. Surface gradients as high as  $\sim 75^\circ$  are observed in the STM image and correlate to regions of the BEEM image with an  $\sim 85\%$  reduction in the BEEM current.

attenuation length in the metal and the transmissivity through the semiconductor depletion region are temperature dependent is expected since the phonon populations in both regions should decrease as a function of temperature. To estimate the relative interaction lengths of both elastic and inelastic scattering events in the metal overlayer, both the temperature and the energy dependence of  $\lambda_q$  must be taken into account. Assuming that the contribution of multiply scattered electrons to the BEEM current can be neglected,

the attenuation length of the BEEM electrons in the metal overlayer can be expressed as  $1/\lambda_a = 1/\lambda_i + 1/\lambda_{ph} + 1/\lambda_d$ , where  $\lambda_i$  is the path length for inelastic electron-electron scattering,  $\lambda_{ph}$  is the path length for acoustic-phonon scattering, and  $\lambda_d$  is the path length for defect scattering. Since sharply reduced BEEM currents at regions of large gradients in the surface topography have been observed, this strongly suggests that this approximation is valid. The probability for inelastic electron-electron scattering is theoretically predicted to have a  $(E + E_F)/E^2$  dependence, where  $E_F$  is the Fermi energy of the metal.<sup>23</sup> This should result in a decrease in  $\lambda_i$  of  $\sim 40\%$  over the energy range 0.9–1.2 eV. Therefore, the lack of energy dependence for  $\lambda_a$  indicates that the path length for elastic scattering events is considerably smaller than that for electron-electron scattering. The value of  $\lambda_{ph}$  is expected to be approximately equal to the conductivity mean free path of pure bulk Au, which is 417 Å at 273 K and 1668 Å at 77 K.<sup>24</sup> Since the measured value of  $\lambda_a$  is only 133 Å at RT, and a relatively small 11% increase in this value is measured at 77 K, this indicates that the scattering in the metal overlayer is primarily dominated by elastic scattering from defect sites.

One might be tempted to conclude that the measurement of a smaller value for  $\lambda_e$  than  $\lambda_i$  should result in diffuse transport through the metal overlayer. However, the actual magnitude of  $\lambda_e$ , which is required for transition to the diffuse transport regime, is difficult to determine from first principles.<sup>14</sup> Our experimental observation of the search-light effect, as well as previously published BEEM results for Au/Si interfaces<sup>8,21</sup> which have measured nanometer resolution at the *M-S* interface for similar Au overlayer thicknesses, indicate that the electron transport is ballistic. In other words, once an electron is deflected from its original trajectory by an elastic scattering event, the probability of it eventually crossing the *M-S* interface without undergoing an inelastic scatter is still quite low for the defect density of these films.

Since RT-grown Au/Si(100) is a nonepitaxial system with a very large lattice mismatch ( $\sim 25\%$ ), it is expected that the metal overlayer will have a very large defect density during the first several layers of growth. In fact, a previous AES/LEED study<sup>18</sup> of Au/Si interface growth at RT has indicated that gold silicide is present in the overlayer, and that no long-range order is observed with LEED for coverages up to  $\sim 100$  Å. Beyond this coverage, no gold silicide was detected, and diffuse ring structures which transformed to distinct multidomain (111) LEED spots by a coverage of  $\sim 300$  Å were observed. This growth morphology may also partially explain the large discrepancy of the value of  $\lambda_a$  measured by BEEM and by internal photoemission since the Au film thicknesses measured in the internal photoemission studies were considerably larger than those measured in this study. In fact, Ludeke and Bauer<sup>11</sup> have come to a similar conclusion for the large discrepancy between the value of  $\lambda_a$  that they measure for Pd/Si with BEEM (31 Å at 1 eV) and the value measured by internal photoemission (170 Å at 0.85 eV).<sup>2</sup> For epitaxial systems where the metal overlayer defect density can be more carefully controlled, there should be better agreement between the attenuation lengths measured by BEEM and internal photoemission. Attenuation length measurements at 77 K for the *epitaxial* CoSi<sub>2</sub>/Si(111) inter-

face have resulted in values of  $\lambda_a = 70$  Å by BEEM spectroscopy<sup>25</sup> and  $\lambda_a = 90$  Å by internal photoemission<sup>26</sup> at an energy of 0.8 eV, which gives credence to this model.

The measurement of almost twice the transmissivity through the depletion region of the Si at 77 K is in direct contradiction with previous analytical calculations which predicted only an  $\sim 15\%$  increase in the transmissivity for Au/Si at 77 K.<sup>27,28</sup> Both studies modeled the temperature-dependent collection efficiency in the depletion region as due to electron interactions with the 63-meV transverse optical phonons in Si. However, all semiconductors with the diamond structure have a low-frequency transverse acoustic-phonon branch which has an anomalously flat dispersion away from the zone center that results from the strong coupling of the lattice ions with the electronic states in the semiconductor.<sup>29</sup> It is expected that electrons over the energy range measured in this study should have a significant probability for interaction with these thermally excited transverse acoustic phonons.<sup>30</sup> In addition, the transverse acoustic-phonon energy of  $\sim 20$  meV for Si (Ref. 31) is small enough to expect a significant population of this mode at RT. Since the models used in the previously mentioned analytical calculations only considered electron scattering with optical phonons, the neglecting of acoustic-phonon scattering modes is the most probable origin of the large discrepancy. This large coupling of the electrons to the acoustic phonon modes may also partially account for the similarities of BEEM spectroscopy data for both the Si(100) and Si(111) surfaces, since phonon scattering events before the Schottky-barrier maximum would provide an additional source of transverse momentum. However, the relative importance of this effect, when compared to scattering at the interface which results from the nonepitaxial nature of the Au/Si system, cannot be determined at this time since temperature-dependent BEEM measurements on the Au/Si(111) have not been performed.

The observation of nearly featureless BEEM images of Au/Si(100) by several groups is most certainly an effect of tip apex geometry. Although we have obtained images which show clear evidence for the search-light effect, the great majority of images taken with both Au and Pt-Ir tips also do not show this effect. In addition, the lifetime of the tips with an apex that allows imaging of the search-light effect are typically limited to a fraction of a BEEM scan (a typical BEEM scan takes  $\sim 15$  min for our microscope). This is presumably due to the delicate nature of such a sharp protrusion. Since the yield strength of Pt-Ir is approximately twice that of Au, the superior mechanical stability of Pt-Ir tips during imaging is not unexpected. Although the quality of Au tips for imaging was found to be inferior to Pt-Ir tips, the contrary was true for spectroscopy. Tip contamination problems were not encountered very often for either Au or Pt-Ir tips at RT; however, large instabilities in the tunneling current were often observed when using Pt-Ir tips at 77 K. Therefore, all of the spectroscopy data reported in this paper were taken using Au STM tips.

Although the tip apex geometry is found to play a major role in the observed BEEM topography, sample preparation procedure might also explain some of the discrepancies observed for different groups studying Au/Si interfaces. Ideally, preparing samples under UHV conditions should provide the most controlled, contamination-free interfaces. However,

great care must be taken to ensure that the Au source is properly outgassed before deposition, since Si is a very reactive surface. For Si samples prepared by a wet chemical etch before Au deposition, contamination problems during deposition are reduced since the Si surface is left with a hydrogen passivation layer.<sup>32</sup> On the other hand, contamination problems can occur during the etching process itself if the composition of the etching solution is not carefully controlled. Since PES studies have indicated that a gold silicide surface segregation layer exists during the initial stages of overlayer growth,<sup>10,33</sup> it is expected that this silicide layer would have an adverse effect on BEEM imaging performed in air due to the formation of an insulating SiO<sub>2</sub> overlayer. No indication of this effect has been observed for the samples prepared in this study, which either indicates that the silicide is effectively buried for the range of sample thicknesses measured in this study or that the hydrogen passivation layer prevents the formation of the silicide layer.

## VI. CONCLUSIONS

The lack of energy dependence and the relatively small temperature-dependent change in  $\lambda_a$  that has been measured with BEEM are consistent with the dominance of electron scattering from defects over the range of Au overlayers measured in this study. In addition, the large discrepancy between the values of  $\lambda_a$  measured by BEEM and internal photoemission for Au/Si samples has been primarily attributed to the different growth morphology of Au at the higher coverages measured in the internal photoemission studies. Our transport measurements, which have determined that almost half of the electrons which pass into the Si depletion region are scattered back into the metal region at RT due to phonon

absorption, indicate that previously published analytical calculations<sup>27,28</sup> have underestimated the importance of hot-electron interactions with the acoustic phonon modes in the Si.

The measurement of the search-light effect for Au/Si(100) gives strong evidence that BEEM electron transport through the metal overlayer is essentially ballistic, i.e., the trajectory of the injected electrons through the Au overlayer remains unchanged, at energies up to 1.2 eV and for overlayer thicknesses up to a few hundred Å. The observation of featureless BEEM images by previous groups has been attributed to the need of an extremely sharp tip apex to see this effect. The good agreement between the experimentally observed and calculated reductions in the BEEM current using a model which assumes that the transmission is independent of the incident angle indicates that a violation of transverse momentum conservation results from scattering at the metallurgical interface.

## ACKNOWLEDGMENTS

Special thanks is given to Professor N. John DiNardo for informative discussions on electron scattering mechanisms at metal-semiconductor interfaces, and to Professor Gene Melé for in depth discussions on electron-phonon interactions in Si. In addition, we would like to thank Wolf Nadler for the technical support that he provided in the design of the BEEM electronics, and Hitesh Dholakia and Anthony Chan for the assistance that they provided in the development of our BEEM imaging software. This work is supported in part by the U.S. Air Force through Rome Laboratories at Hanscom AFB and the Office of Naval Research (ONR).

\*Present address: Department of Physics, Indian Institute of Science, Bangalore, India 560012.

<sup>1</sup>C. R. Crowell and S. M. Sze, in *Physics of Thin Films*, edited by G. Hass and R. F. Thun (Academic, New York, 1967), Vol. 4, p. 325.

<sup>2</sup>C. R. Crowell, W. G. Spitzer, L. E. Howarth, and E. E. LaBate, *Phys. Rev.* **127**, 2006 (1962).

<sup>3</sup>S. M. Sze, J. L. Moll, and T. Sugano, *Solid-State Electron.* **7**, 509 (1964).

<sup>4</sup>R. W. Soshea and R. C. Lucas, *Phys. Rev.* **138**, A1182 (1965).

<sup>5</sup>L. D. Bell and W. J. Kaiser, *Phys. Rev. Lett.* **61**, 2368 (1988).

<sup>6</sup>L. J. Schowalter and E. Y. Lee, *Phys. Rev. B* **43**, 9308 (1991).

<sup>7</sup>E. Y. Lee, B. R. Turner, L. J. Schowalter, and J. R. Jimenez, *J. Vac. Sci. Technol. B* **11**, 1579 (1993).

<sup>8</sup>H. Palm, M. Arbes, and M. Schulz, *Phys. Rev. Lett.* **71**, 2224 (1993).

<sup>9</sup>A. Fernandez, H. D. Hallen, T. Huang, R. A. Buhrman, and J. Silcox, *Appl. Phys. Lett.* **69**, 2679 (1990).

<sup>10</sup>M. T. Cuberes, A. Bauer, H. J. Wen, D. Vandr e, M. Prietsch, and G. Kaindl, *J. Vac. Sci. Technol. B* **12**, 2422 (1994).

<sup>11</sup>R. Ludeke and A. Bauer, *Phys. Rev. Lett.* **71**, 1760 (1993).

<sup>12</sup>A. Bauer, M. T. Cuberes, M. Prietsch, and G. Kaindl, *Phys. Rev. Lett.* **71**, 149 (1993).

<sup>13</sup>M. Prietsch and R. Ludeke, *Phys. Rev. Lett.* **66**, 2511 (1991).

<sup>14</sup>E. Y. Lee, Ph.D. dissertation, Rensselaer Polytechnic Institute, 1992.

<sup>15</sup>A. Bauer and R. Ludeke, *Phys. Rev. Lett.* **72**, 928 (1994).

<sup>16</sup>W. J. Kaiser and R. C. Jaklevic, *Surf. Sci.* **55**, 181 (1987).

<sup>17</sup>Lake Shore Cryotronics, C-1 coax cable, part No. 9002-002-025.

<sup>18</sup>K. Oura and T. Hanawa, *Surf. Sci.* **82**, 202 (1979).

<sup>19</sup>P.-H. Chang, G. Berman, and C. C. Chen, *J. Appl. Phys.* **63**, 1473 (1988).

<sup>20</sup>H. J. Mamin, P. H. Guethner, and D. Rugar, *Phys. Rev. Lett.* **65**, 2418 (1990).

<sup>21</sup>A. M. Milliken, S. J. Manion, W. J. Kaiser, L. D. Bell, and M. H. Hecht, *Phys. Rev. B* **46**, 12 826 (1992).

<sup>22</sup>H. Palm, M. Arbes, and M. Schulz, *Appl. Phys. A* **56**, 1 (1993).

<sup>23</sup>J. J. Quin, *Phys. Rev.* **126**, 1453 (1962).

<sup>24</sup>N. W. Ashcroft and N. D. Mermin, *Solid State Physics* (Saunders, Philadelphia, 1976).

<sup>25</sup>E. Y. Lee, H. Sirringhaus, and H. von K anel, *Surf. Sci.* **314**, L823 (1994).

<sup>26</sup>J. Y. Duboz and P. A. Badoz, *Phys. Rev. B* **44**, 8061 (1991).

<sup>27</sup>C. R. Crowell and S. M. Sze, *Solid-State Electron.* **8**, 979 (1965).

<sup>28</sup>E. Y. Lee and L. J. Schowalter, *J. Appl. Phys.* **70**, 2156 (1991).

<sup>29</sup>W. Weber, *Phys. Rev. Lett.* **33**, 371 (1974).

<sup>30</sup>E. J. Mel e (private communication).

<sup>31</sup>H. Palevsky, D. J. Hughes, W. Kley, and E. Tunkelo, *Phys. Rev. Lett.* **2**, 258 (1959).

<sup>32</sup>H. Ubara, T. Imura, and A. Hiraki, *Solid State Commun.* **50**, 673 (1984).

<sup>33</sup>J.-J. Yeh, J. Hwang, K. Bertness, D. J. Friedman, R. Cao, and I. Lindau, *Phys. Rev. Lett.* **70**, 3768 (1993).